Contemporary Mathematics
http://ojs.wiserpub.com/index.php/CM/

Research Article

Peristaltic Transport of a Jeffrey Nanofluid in a Vertical Layer with Suction and Injection: Effect of Velocity No-Slip, Temperature and Concentration with Application

S. Sivaranjani, A. Kavitha*

Department of Mathematics, School of Advanced Sciences, Vellore Institute of Technology, Vellore, 632014, India
E-mail: kavitha@vit.ac.in

Received: 4 July 2024; **Revised:** 19 August 2024; **Accepted:** 26 September 2024

Abstract: This study explores the peristaltic motion of a Jeffrey nanofluid in a vertical channel, as well as the effects of suction and injection at the walls. The non-Newtonian behavior of the fluid is described using the Jeffrey fluid model. Which includes both relaxation and retardation times. Nanoparticles are used to improve the fluid's thermal conductivity and overall heat transfer qualities. The governing equations, such as continuity, momentum, energy, and nanoparticle concentration, are based on incompressible and laminar flow assumptions. Peristaltic flow has been extensively employed for a range of biological fluids, with a particular emphasis on non-Newtonian fluids due to their industrial implications. The intricacy of non-Newtonian fluids has led to the development of numerous models, including the Jeffrey fluid. Model which is one of the simplest linear models that accurately capture non-Newtonian properties, making it suitable for analytical solutions. Nanofluids, which consist of nanoparticles dispersed in a base fluid, are innovative materials. With numerous applications in engineering, biology, medicine, and other fields. These fluids have unique properties that make them particularly useful in a range of applications. The resulting partial differential equations are mathematically turned into dimensionless by applying appropriate transformations. The results demonstrate that peristaltic waves have significant influence on velocity and temperature, and nanoparticles improve thermal conductivity, which increases heat transfer rate, yet the elasticity of Jeffrey fluid gives unique flow features. Using MATLAB software, the effects of all physical factors on temperature, velocity, and concentration fields are visually investigated.

***Keywords*:** peristaltic transport, Jeffrey fluid, suction and injection

MSC: 76Z10, 76A05, 76D05

1. Introduction

The study of fluid flow caused by peristaltic motion is of great interest in many scientific and technical domains due to its importance in biological systems and industrial applications. Peristalsis is defined as the wave-like contractions and relaxations of the walls of a flexible tube that propagate down its length to cause fluid flow. This mechanism is used in many physiological processes, including the passage of food through the gastrointestinal system and the transfer of urine via the ureters. Peristaltic pumps are commonly employed in engineering to handle corrosive, viscous, or shear-sensitive fluids that must be kept clean. Jeffrey fluid substantially contributes to the understanding and use of peristaltic

DOI: https://doi.org/10.37256/cm.5420245254

motion by offering a realistic model that incorporates the viscoelastic properties of many real-world fluids. Its capacity to store and release energy, improve mixing, effectively disperse stress, and allow regulated suction and injection operations makes it important for understanding biological fluid movement and enhancing industrial applications. Nanofluids are designed colloidal suspensions of nanoparticles (ranging from 1 to 100 nm) in a base fluid. They have superior thermal characteristics as compared to their base fluids, making them very desirable for heat transfer applications. Expressions are created for the fields velocity, temperature, concentration, and stream function. Akbar et al. [1] demonstrated that a magnetohydrodynamic (MHD) Jeffrey nanofluid moved in mixed convective and peristaltic motion in an asymmetric channel with Newtonian thermal expansion. Reddy et al. [2] examined the peristaltic Motion of a power-law fluid in an asymmetric Channel. Weinberg [3] investigated the theoretical and experimental treatment of peristaltic pumping and its relationship with ureteral function. Berman et al. [4] toured laminar flow in tubes with porous walls. Mishra et al. [5] explored the peristaltic slip flow in a porous tube with a porous outer layer. Noreen et al. [6] investigate the effect of slip and produced magnetic fields on the peristaltic flow of pseudoplastic fluid. Channabasappa et al. [7] examined the impact of a porous liner on flow between two concentric rotating cylinders. Usman et al. [8] influenced the effect of magnetic Field and Chemical Reaction on Unsteady Natural Convective Flow in a Vertical Porous Channel. Shojaefard et al. [9] investigated suction/injection to regulate fluid flow on the surface of subsonic aircraft. Brasseur et al. [10] explored the effect of a peripheral layer of varying viscosity on peristaltic pumping using Newtonian fluid. Chandra et al. [11] reviewed pulsatile flow in circular tubes with different cross-sections using suction/injection. Qadeer et al. [12] it's effort looked at irreversibility in nanofluid flow in converging and diverging channels. They analyzed flow in two dimensions. That was steady and incompressible. The nanofluid was made up of water and aggregates.

Kumar et al. [13] observed fluid flow behavior that differed from Darcy's law in a conduit that narrowed and expanded. They especially investigated how carbon nanotubes affect this non-Darcian flow. This study most likely sought to determine how the presence of carbon nanotubes influence fluid flow patterns in channels of varied diameters. Anuar et al. [14] evaluated nanofluids, which have lately gained substantial importance in a variety of industries such as vehicle manufacturing, electronics cooling, catalytic processes, smart computer technologies, solar energy applications, transportation, and biological research. These nanofluids have higher heat transmission efficiency than standard fluids, making them useful for boosting performance and efficiency in a variety of applications. Rasool et al. [15] examined the properties of a kind of fluid known as Jeffrey nanofluid. They focused primarily on how this nanofluid behaved as it flowed over a stretched surface. The Researchers also used the Darcy-Forchheimer relation, which defines the resistance to fluid flow in porous media. Swain et al. [16] examined the MHD flow of a Newtonian fluid across a sheet of elastic in a porous matrix. Considered viscous dissipation and joule heating (ohmic heating). Hussein et al. [17] investigated the non-linear transport of peristaltic fluid. In the presence of oxytactic organisms in a horizontally uniform/non-uniform tunnel filled with Jeffrey non-Newtonian nanofluids. The significance of linear electromagnetic radiation, viscous dissipation, and electrical magnetic fields is discussed. Peristaltic transport of a nanofluid in a vertical channel is a fascinating topic with significant applications in both biomedical and industrial fields. This process involves the movement of a nanofluid, which is a fluid containing nanoparticles, through a channel due to the peristaltic waves generated by the walls of the channel studied by Haseena et al. [18]. Tayebi et al. [19] used the finite element method to model free convection. Caused by double-diffusion with Soret/Dufour effects of nano-encapsulated phase change materials (PCMs) in an I-Shaped enclosure with a novel type of corrugated vertical walls under Neumann thermal and solutal conditions. Dogonchi et al. [20] investigated the effects of viscous dissipation, thermal radiation, and joule heating on the squeezing flow current and heat transfer mechanism of a magnetohydrodynamic nanofluid flow in parallel discs during a suction/blowing operation. The results Look at how the radiation parameter, suction/blowing parameter, magnetic parameter, squeezing number, and nanoparticle concentration affect heat transfer and flow field. Tirth et al. [21] discussed how double-diffusive convection has several relevant technical applications. These applications include electronic apparatus cooling, drying operations, fuel cells, geothermal engineering, and thermal storage. They conduct an entropy-thermal study of magnetised Boussinesq-free double-diffusive convection caused by internal heat and a concentration source block in a nanofluid-filled c-shaped inclined restricted space. Nayak et al. [22] examined the hydrothermal features of fluid flow within a hexagonal enclosure, which are extremely important because to their wide-ranging applicability in many fields. Despite their potential significance, there is currently little understanding of free convection flow in these geometries. Dogonchi

et al. [23] investigated thermic energy storage devices based on nano-encapsulated phase change material and a complex charger within the storage system. The cavity inclination angle and inner heater structure can be useful characteristics for controlling heat transmission and entropy formation. Rafiq et al. [24] examined the peristaltic mobility of Jeffrey nanofluid via an asymmetric, tapered conduit in the presence of a magnetic field. The fundamental motivation for this research is to investigate the heat transfer capacities of nanofluids for the treatment of a variety of disorders, including cancer. We can so conclude that this study can lay the groundwork for comprehending the physiological system through electroosmotic events. It has fascinating applications, including the delivery of pharmaceuticals and food diagonists. Pasha et al. [25] explained the modelling and the numerical simulation of natural convective flow, heat exchange, and entropy generation features within a hexagonal-shaped domain influenced by an inclined magnetic field and filled with a non-Newtonian shear-thickening fluid charged with alumina nanoparticles. Three variant configurations of three cooling channels positioned inside the domain are considered. Micropolar fluids are liquids whose behaviour is influenced by the microrotation of substructure particles. Seyyedi et al. [26] study the natural convection flow of a micropolar nanofluid (Al_2O_3, water) in a semi-annulus enclosure with an angled magnetic field. Pasha et al. [27] investigated the efficacy of exothermic reaction on the thermal behavior of suspension of Nano-Encapsulated phase change materials particles in a complex adiabatic enclosure which entails two differently heated circular cylinders. These cylinders have the potential to move horizontally and to rotate clockwise. This study aims to assess the effects of transmitted mass and heat on Jeffrey nanofluid Magneto-Hydrodynamic peristaltic contraction via a porous medium with inclined symmetric channels.

This study aims to assess the effects of transmitted mass and heat on Jeffrey nanofluid Magneto-Hydrodynamic peristaltic contraction via a porous medium with inclined symmetric channels. Thus, the walls of which are caused by peristaltic motion in porous materials investigated by Abd-Alla et al. [28] ploting graphs were utilized to evaluate the effects of the appropriate variables on the aforementioned numbers based on the results of the computation. The findings demonstrate that the conditions have a considerable influence. Shao et al. [29] investigated natural convection heat transfer in a porous prismatic enclosure emplacing. Two movable heated baffles could be used in this study. The domain may be loaded with ternary hybrid nanofluid, and the governing energy and Navier-Stokes equations may be solved using a finite element method. Li et al. [30] investigated the thermal performance and flow properties of hybrid nanofluids, specifically those containing iron oxide and copper nanoparticles, in a Casson fluid model with hall current effects. Fluids comprising two types of nanoparticles: iron oxide (Fe_3O_4) and copper. Hybrid nanofluids are designed to improve thermal conductivity and other attributes over single-component nanofluids. A channel with wavy or undulating form adds complexity to flow and heat transfer operations. Bafakeeh et al. [31] provide valuable insights into the biconvective characteristics of viscoelastic micropolar nanofluids, taking into account varying thermal conductivity and thermos-diffusion effects. It advances our understanding of complex fluid behaviours in viscoelastic micropolar nanofluids, which is critical for building and optimising sophisticated thermal systems. Turkyilmazoglu [32] explored the recent advancements in the study of peristalsis and fluid dynamics have provided insignificant insights. For instance, the corrections to the long wavelength approximation in the study of peristalsis viscous fluid flow within a wavy channel have been explored in a study. Rahman et al. [33] investigated unsteady three-dimensional MHD flow of nanofluids over a decelerated rotating disks with a uniform magnetic field has been comrehensively analyzed, shedding light on the behavior of nanofluids under these conditions. Siddiqui et al. [34] investigated into the film flow of nano-micropolar fluid, considering dissipation effects, offers valuable contributions to the understanding of such complex systems. The no slip condition, which states that the fluid velocity at the boundary of a solid surface is equal to the velocity of the surface itself (usually zero for a stationary border), provides numerous advantages in the setting of Jeffrey nanofluids in a vertical channel with peristalsis. Here are a few advantages and reasons why the no-slip criterion is important: Improved predictability and stability of flow: The no-slip condition creates a well-defined boundary layer, making it easier to predict and model flow behaviour, resulting in more stable and accurate simulations and designs. Slip-Induced Instabilities Prevention: In many practical applications, boundary slip can cause flow instabilities and abnormalities. The no-slip condition contributes to maintaining a steady flow regime, which is necessary for consistent and reliable functioning. After undergoing a nonlinear deformation, tensions emerge in the streamlines, and the microstructure takes time to relax. The Jeffrey fluid model well explains how the tension in the stream lines causes non-zero ordinary stresses inside the fluid. Some examples of these flows include reverse osmosis-driven desalination, transpiration cooling, ultrafiltration

in the kidney glomeruli, fluid reabsorption via the porous wall of the renal proximal tubule, and blood filtering during haemodialysis in an artificial kidney. According to certain experimental studies, typical tension at a border. The purpose of this study is to look into the peristaltic system of a Jeffrey nanofluid in a vertical tube influenced by suction and injection.

2. Mathematical formulation

In a vertical layer, the long wavelength and low Reynolds number approximation for a Jeffrey nanofluid's two-dimensional peristaltic motion are discussed. The channel has a consistent width of $2a$, as shown in the Figure 1. The x-axis corresponds to the channel's centreline but opposes the gravitational acceleration vector g. The channel walls are perpendicular to the y axis. A sinusoidal wave train travels down the channel walls at a constant speed of c. Fluid is injected into the channel from the lower wall and removed from the top wall at the same velocity, v_0.

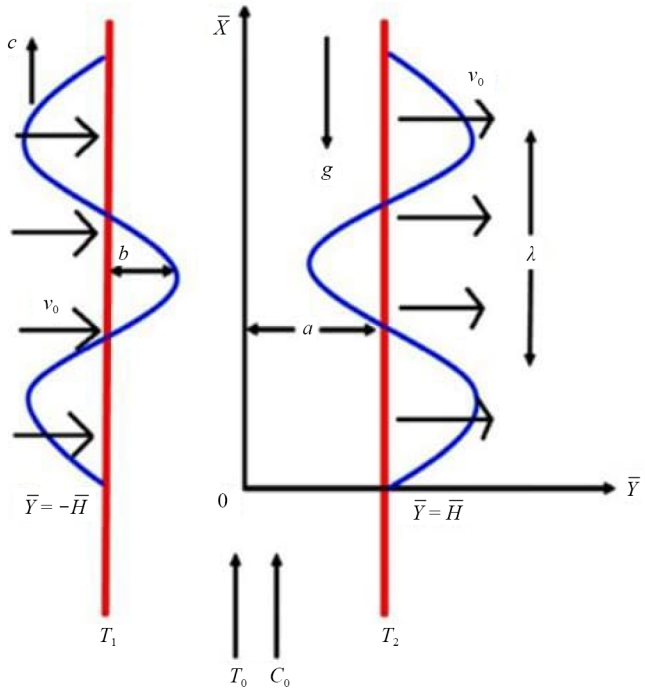

Figure 1. Physical model

The wall deformation equation is given by [35].

$$\bar{y} = \bar{H}(\bar{X}, t) = a + b\sin\frac{2\Pi}{\lambda}(\bar{X} - ct). \tag{1}$$

Boundary conditions at the $(\bar{y} = -\bar{H})$ walls: Concentration: (C1). Temperature: (T1). At the $(\bar{y} = -\bar{H})$ walls: Concentration: (C2). Temperature: (T2). Conservation equations: The conservation equations guiding the flow are: Mass Conservation: Ensures that the rate of mass change inside the fluid element matches the net mass input into the element. Momentum conservation describes how fluid particles' momentum varies as a result of forces acting on them. Energy Conservation (Thermal Energy): Includes heat addition and labor done on fluid particles. Nanoparticle concentrations are

specific to the presence of nanoparticles. Oberbeck Boussinesq approximation: A model for buoyancy effects in a fluid of variable temperature or composition [36].

$$\nabla.\bar{v} = 0. \tag{2}$$

$$\rho_f(\bar{v}.\nabla v) = -\nabla p + \mu\left[\frac{1}{1+\lambda}\right]\nabla^2\bar{v} - \rho v_0\frac{\partial u}{\partial y} + \{c\rho_p + (1-c)*[\rho_f.(1-\beta(T-T_0))]\}g. \tag{3}$$

$$(\rho c_f)(\bar{v}.\nabla T) = k_B.\nabla^2 T + (\rho c)_p\left[D_B\nabla T.\nabla c + \left(\frac{DT}{T_0}\right)\nabla T.\nabla T\right]. \tag{4}$$

$$\bar{v}.\nabla c = D_B\nabla^2 c + \left(\frac{D_T}{T_0}\right)\nabla^2 T. \tag{5}$$

Reference nanoparticle volume concentration is defined by $C_0 = \frac{(c_1+c_2)}{2}$, reference temperature is represented by $T_0 = \frac{(T_1+T_2)}{2}$, fluid heat capacity is expressed by $(\rho C)_f$, nanoparticle mass density is given by $(\rho)_p$, and the optimum heat capacity of the nanoparticles material is represented by $(\rho C)_p$. The linearized momentum equation (2) is calculated using the Oberbeck-Boussinesq approximation, which assumes a dilute nanoparticle concentration and an adequate reference pressure.

$$\rho_f(\bar{v}.\nabla v) = -\nabla p + \mu\left[\frac{1}{1+\lambda_1}\right]\nabla^2\bar{v} + [(\rho_p - \rho_{f_0})(C-C_0) - (1-C_0)\rho f_0\beta(T-T_0)]g - \rho v_0\frac{\partial u}{\partial y}. \tag{6}$$

$$\bar{v} = 0,\ \frac{\partial u}{\partial \bar{x}} = 0,\ \frac{\partial T}{\partial \bar{x}} = 0,\ \frac{\partial c}{\partial \bar{x}} = 0,\ \frac{\partial \bar{p}}{\partial \bar{y}} = 0,\ \frac{\partial \bar{p}}{\partial \bar{x}} = \frac{d\bar{p}}{d\bar{x}} = \text{constant}. \tag{7}$$

Thus, Equations (2) through (7) become,

$$-\frac{d\bar{p}}{d\bar{x}} + \mu\left[\frac{1}{1+\lambda_1}\right]\frac{d^2\bar{u}}{d\bar{y^2}} - \frac{du}{dy}\rho v_0 + [(1-C_0)\rho f_0\beta(T-T_0) - (\rho_f - \rho f_0)(C-C_0)]g = 0. \tag{8}$$

$$K_B\frac{d^2T}{d\bar{y}^2} + (\rho c)_p\left[D_B\frac{dc}{d\bar{y}}\frac{dT}{d\bar{y}} + \left(\frac{D_T}{T_0}\right)\left(\frac{dT}{d\bar{y}}\right)^2\right] = 0. \tag{9}$$

$$D_B\frac{d^2c}{dy^2} + \left(\frac{D_T}{T_0}\right)\frac{d^2T}{d\bar{y}^2} = 0. \tag{10}$$

The suitable boundary conditions are as follows [18]:

$$\bar{u} = -c,\ T = T_1,\ C = C_1,\ \text{at } \bar{y} = -\bar{H}. \tag{11}$$

$$\bar{u} = -c,\ T = T_2,\ C = C_2,\ \text{at } \bar{y} = \bar{H}.$$

The pressure differential at the channel ends has been determined to be constant, the flow is steady in the wave frame $(\bar{x},\ \bar{y})$, and it becomes instantaneously unstable in the laboratory frame $(\bar{X},\ \bar{Y})$. The channel length is an integral multiple of the wavelength. The transformation between these two frames is provided by,

$$\bar{x} = \bar{x} - c\bar{t},\ \bar{y} = \bar{Y},\ \bar{u} = \bar{U} - c,\ \bar{v} = \bar{V},\ \bar{p} = \bar{P}(x,\ t).$$

The non-dimensional quantity that follows is utilised:

$$x = \frac{\bar{x}}{\lambda},\ y = \frac{\bar{y}}{a},\ u = \frac{\bar{u}}{c},\ p = \frac{\bar{p}a^2}{\mu\lambda c},\ h = \frac{\bar{H}}{a},\ \phi = \frac{b}{a},\ t = \frac{c\bar{t}}{\lambda},\ T = \theta(T_2 - T_0) + T_0,\ C = \sigma(C_2 - C_0),\ p = -\frac{dp}{dx},$$

$$Gr = \frac{(1-c_0)g\beta(T_2-T_0)a^3}{v^2},\ Nr = \frac{g(\rho_f - \rho_{f_0})(c_2-c_0)a^2}{\mu c},\ Re = \frac{\rho ac}{v},\ Nb = \frac{D_B(c_2-c_0)}{\frac{k_B}{(\rho c)_p}},\ Nt = \frac{D_T(T_2-T_0)}{\frac{T_0 k_B}{(\rho c)_p}}. \tag{12}$$

In this case, the reference temperature is represented by $T_0 = \dfrac{(T_1+T_2)}{2}$ and the reference nanoparticle concentration is represented by $C_0 = \dfrac{(C_1+C_2)}{2}$.

The non-dimensional form of the governing equations is:

$$\left[\frac{1}{1+\lambda_1}\right]\frac{d^2u}{dy^2} - k\frac{du}{dy} + \frac{Gr}{Re}\theta - Nr\sigma + p = 0. \tag{13}$$

$$\frac{d^2\theta}{dy^2} + Nb\frac{d\theta}{dy}\frac{d\sigma}{dy} + Nt\left(\frac{d\theta}{dy}\right)^2 = 0. \tag{14}$$

$$\frac{d^2\sigma}{dy^2} + \frac{Nt}{Nb}\frac{d^2\theta}{dy^2} = 0. \tag{15}$$

By reducing the boundary conditions (11) to

$$u = -1,\ \theta = -1,\ \sigma = -1,\ \text{at } y = -h = 1 + \sin 2\pi x.$$

$$u = -1,\ \theta = 1,\ \sigma = 1,\ \text{at } y = h = 1 - \sin 2\pi x + \phi. \tag{16}$$

In this case, the Pressure Parameter is delimited by, $p = \dfrac{dp}{dx}$ the Grashof number by Gr, and the Reynolds number by Re. The mixed convection parameter is represented as Nr is the buoyancy-ratio parameter. Nb indicates the Brownian motion parameter, Nt specifies the thermophoresis parameter, and Jeffrey parameter is denoted by λ_1.

3. Solution of the problem

Using boundary conditions (16), analytical calculations for concentration, temperature, velocity, and axial pressure gradient are produced from equations (13)-(15).

$$\theta(y) = S_3 + S_4 e^{-S_2 y}. \tag{17}$$

$$\sigma(y) = -\frac{Nt}{Nb}\theta + S_1 y. \tag{18}$$

$$u(y) = -1 - S_8\left(\frac{2hp}{k}\right)e^{k(1+\lambda_1)h} - S_8 S_9 e^{k(1+\lambda_1)h} - \frac{hp}{k} + \frac{S_5 e^{-S_2 h}h(1+\lambda_1)}{S_2^2 + K(1+\lambda_1)S_2} - S_6\frac{h}{k}$$
$$+ S_8\left(\frac{2hp}{k}\right)e^{k}(1+\lambda_1)y + S_8 S_9 e^{k(1+\lambda_1)y} + \frac{yp}{k} - \frac{S_5 e^{-S_2 y}(1+\lambda_1)}{S_2^2 + K(1+\lambda_1)S_2} + S_6\frac{y}{k}. \tag{19}$$

$$P = \frac{1}{S_{11}}\left[q + h + S_8 S_9 e^{k(1+\lambda_1)h}h - \frac{S_5 e^{-S_2 h}h(1+\lambda_1)}{S_2^2 + k(1+\lambda_1)S_2}\right.$$
$$\left. + S_6\frac{h^2}{k} - S_8 S_9 S_{10} + \frac{S_5(1+\lambda_1)}{S_2^2 + k(1+\lambda_1)S_2}\left(\frac{-e^{-S_2 h}}{S_2} - \frac{1}{S_2}\right) - S_6\frac{h^2}{2k}\right]. \tag{20}$$

Upon integrating Equation (19), the stream function expression is obtained as follows:

$$\psi = -y - S_8\left(\frac{2hp}{k}\right)e^{k(1+\lambda_1)h}y - S_8 S_9 e^{k(1+\lambda_1)h}y - \frac{yhp}{k} + \frac{S_5 e^{-S_2 h}h(1+\lambda_1)}{S_2^2 + k(1+\lambda_1)S_2 y} - S_2\frac{yh}{k}$$
$$+ S_8\left(\frac{2hp}{k}\right)\left(\frac{e^{k(1+\lambda_1)y}}{k(1+\lambda_1)} - \frac{1}{k(1+\lambda_1)}\right) + S_8 S_9\left(\frac{e^{k(1+\lambda_1)}}{k(1+\lambda_1)} - \frac{1}{k(1+\lambda_1)}\right)$$
$$+ \frac{yhp}{k} - \frac{S_5(1+\lambda_1)}{S_2^2 + k(1+\lambda_1)S_2}\left(\frac{-e^{-S_2 y}}{S_2} - \frac{1}{S_2}\right) + S_6\frac{hy}{2k}. \tag{21}$$

Here,

$$S_1 = \frac{1}{h}\left(1 + \frac{Nt}{Nb}\right).$$

$$S_2 = NbS_1.$$

$$S_3 = \frac{e^{S_2 h} + e^{-S_2 h}}{e^{S_2 h - e^{-S_2 h}}}.$$

$$S_4 = \frac{2}{e^{S_2 h} - e^{-S_2 h}}.$$

$$S_5 = S_4\left(\frac{Gr}{Re} + Nr\frac{Nt}{Nb}\right).$$

$$S_6 = -NrS_1.$$

$$S_7 = S_3\left(\frac{Gr}{Re} + \frac{Nr}{Nb}\right).$$

$$S_8 = \frac{1}{(e^{-k(1+\lambda_1)h} - e^k(1+\lambda_1)h)}.$$

$$S_9 = \frac{S_5 e^{-S_2 h} h(1+\lambda_1)}{S_2^2 + k(1+\lambda_1)S_2}(e^{-S_2 h} - e^{S_2 h}) + 2S_6\frac{h}{k}.$$

$$S_{10} = \left(\frac{e^{(k(1+\lambda_1))y}}{k(1+\lambda_1)} - \frac{1}{k(1+\lambda_1)}\right).$$

$$S_{11} = \left[-\frac{S_8(2h^2)e^k(1+\lambda_1)h}{k} - \frac{h^2}{k} + \frac{h^2}{k} + \frac{S_8 2hS_{10}}{k}\right].$$

Here S_1 to S_{11} represents the constant value.
In the fixed frame, the instantaneous volume flow rate can be computed using:

$$Q = \int_0^H \bar{U}(\bar{X},\, \bar{Y},\, t)d\bar{Y}. \tag{22}$$

From equation (22) in a wave frame,

$$q = \int_0^h \bar{u}(\bar{x},\, \bar{y},\, t)d\bar{y}. \tag{23}$$

The definition of non-dimensional volume flow rate Q is the average over one peristaltic wave interval as follows:

$$\bar{Q} = q + \frac{1}{T}\int_0^T Q dt = q + 1. \tag{24}$$

4. Pumping characteristics

The pressure rise per wave-length is obtained by integrating equation (20) in relation to x.

$$\Delta p = \int_0^1 \left(\frac{dp}{dx}\right) dx$$

$$\Delta P = \int_0^1 \frac{1}{S_{11}}\left[q + h + S_8 S_9 e^{k(1+\lambda_1)h} h - \frac{S_5 e^{-S_2 h} h(1+\lambda_1)}{S_2^2 + k(1+\lambda_1)S_2} + S_6\frac{h^2}{k}\right.$$

$$\left. - S_8 S_9 S_{10} + \frac{S_5(1+\lambda_1)}{S_2^2 + k(1+\lambda_1)S_2}\left(\frac{-e^{-S_2 h}}{S_2} - \frac{1}{S_2}\right) - S_6\frac{h^2}{2k}\right] dx. \tag{25}$$

The dimensionless F at the wall across a wavelength is given by,

$$F = \int_0^1 h\left(-\frac{dp}{dx}\right) dx. \tag{26}$$

5. Results and discussion

The primary goal of this part is to discuss physically how emergent factors influenced flow patterns with the aid of graphical examples. For Jeffrey nanofluid, the investigation of friction force, velocity, concentration and fluid temperature is also done inorder to better understand these concepts. The parameters are the brownian motion (Nb), Jeffrey nanofluid (λ_1), Grashof number (Gr), Buoyancy ratio (Nr), Thermophoresis parameter (Nt), Suction/Injection parameter (k). From Figure 2 to 4 display the diffrences in the concentration profile for several parameters, including the amplitude ratio, Brownian motion parameter and thermophoresis parameter. From Figure 2 shows that the nanoparticles concentration friction significantly increases the amplitude ratio then the velocity decreases. The concentration of nanoparticles is increased as a result for various Nb values. From Figure 3 shows the concentration changes. It can see that an increase in the Nb tends to conflicts with the profile of the concentration of Nanoparticles. From Figure 4 shows the increasing the value for thermophoresis parameter then the concentration profile must be decreased. The temperature profile rises significantly of an increase in the thermophoresis parameter because it tends to transfer particles from hotter to cooler areas by creating forces that tend to do so with an increase in Nb. The temperature profile increases while the velocity profile increased for the amplitude ratio ϕ as shown in Figure 5. The temperature increases significantly as shown in Figure 6 Then the thermophoresis parameter is increased and then the concentration must also be increased. The effect of the the thermophoresis parameter Nt on the temperature profile are decreased shown in Figure 7. It has been noted that soret effect, which is also known as the thermoporesis effects decreases temperature. As the brownian motion effect becomes more pronounced this correlates to the efficient migration of nanoparticles from the wall to the fluid, which causes the temperature distribution to significantly increases. Then the amplitude ratio is increases then the temperature profile must also increases. The study of effect of physical parameter for fixed value of mixed convection parameter $Gr/Re = 1{,}000$ on the velocity distribution in a vertical channel. From Figure 8-13 depict the effects of physical characteristic on the fluid

velocity with two dimensional in a vertical channel, including Amplitude ratio, Thermophoresis parameter, Brownian motion, Grashof number, Buoyancy ratio, Suction and Injection parameter, Reynolds number, Jeffrey nanofluid. From Figure 8 depicts the behavior of the fluid velocity as the amplitude ratio varies, increasing the value of amplitude ratio the velocity profile decreases. Now increasing the value of thermophoresis parameter then the velocity profile must also increases is visualized in Figure 9. While increasing the value for brownian motion parameter then the velocity profile must be decreased as shown in Figure 10. From Figure 11 buoyancy ratio (Nr) increases the value then it is increased for the velocity profile. From Figure 12 increases the values of suction and injection parameter then it is increases. Suppose the value must be increased above 100 or 1,000 means the flow must be turbulent for reynolds number. Figure 13 shows the impact of the Jeffrey nanofluid parameter λ_1. The fluid with a significant relaxation time is what distingushes viscoelastic fluids. For a Jeffrey nanofluid, the parameter λ_1 represents the relaxation to retardation time in the lower section of the channel it is discovered that rising λ_1 causes a increased in velocity profile.

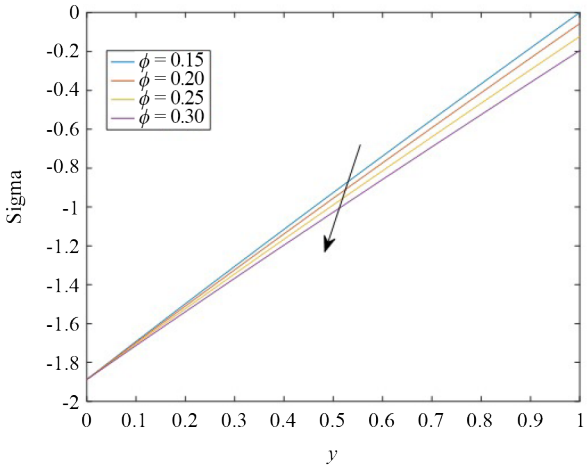

Figure 2. The variation of ϕ in nanoparticle fractions of volume with $Nt = 0.35$, $Nb = 0.45$, $Gr = 0.6$, Re =0.2

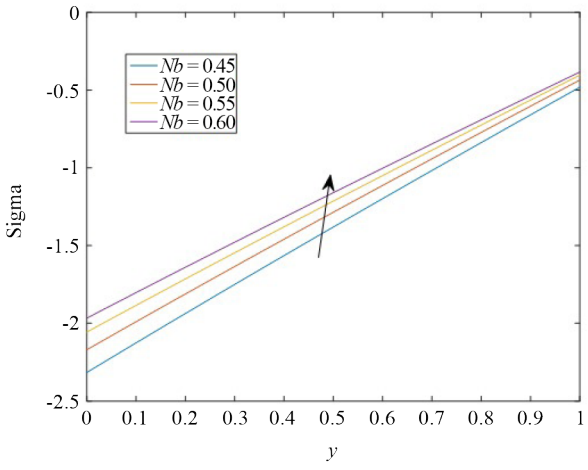

Figure 3. The variation of Nb in nanoparticle fractions of volume with $\phi = 0.30$, $Nt = 0.41$, $Gr = 0.6$, $Re = 0.2$

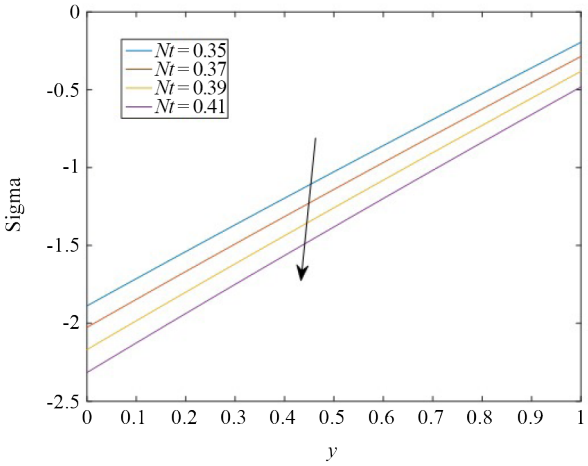

Figure 4. The variation of Nt in nanoparticle fractions of volume with $\phi = 0.30$, $Nb = 0.45$, $Gr = 0.6$, $Re = 0.2$

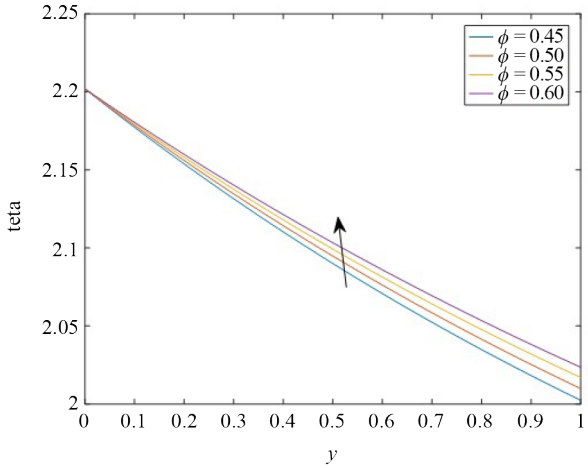

Figure 5. The variation of ϕ in temperature examined with $Nt = 0.31$, $Nb = 0.35$, $Gr = 0.6$, $Re = 0.2$

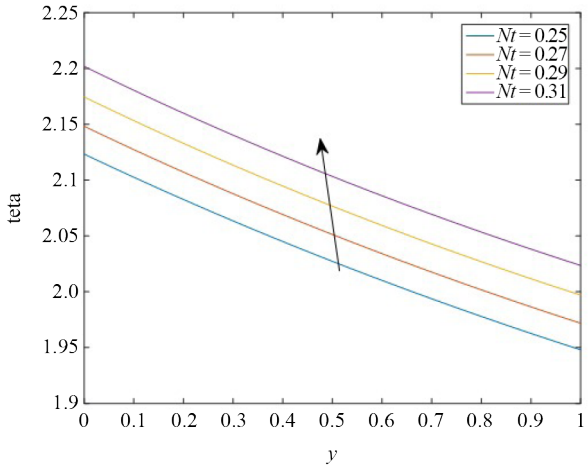

Figure 6. The variation of Nb in temperature examined with $Nt = 0.31$, $\phi = 0.60$, $Gr = 0.6$, $Re = 0.2$

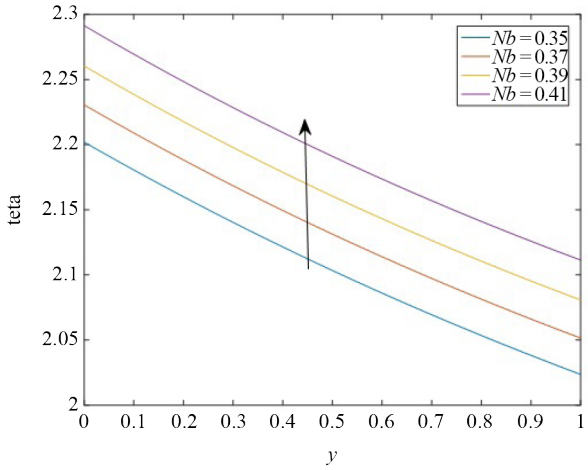

Figure 7. The variation of Nt in temperature examined with $Nb = 0.35$, $\phi = 0.60$, $Gr = 0.6$, $Re = 0.2$

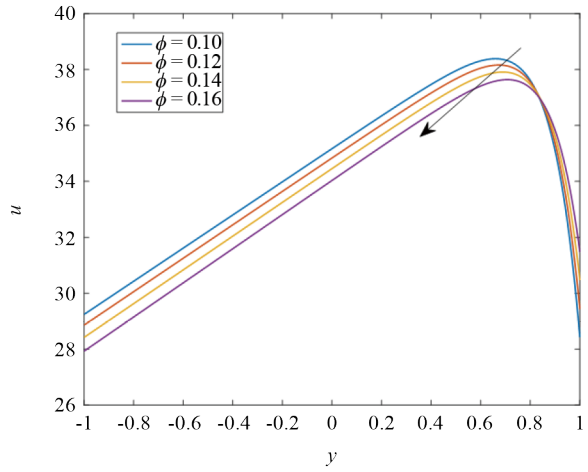

Figure 8. The difference in velocity for various ϕ with $Nt = 0.08$, $Nb = 0.68$, $Nr = 0.28$, $k = 0.54$, $\lambda_1 = 0.58$

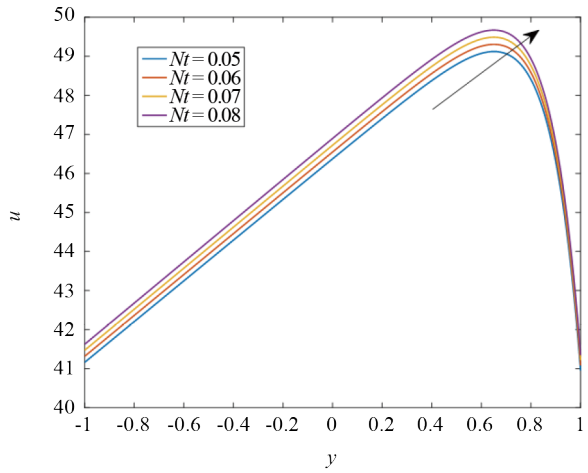

Figure 9. The difference in velocity for various Nt with $\phi = 0.10$, $Nb = 0.25$, $Nr = 0.25$, $k = 0.5$, $\lambda_1 = 0.6$

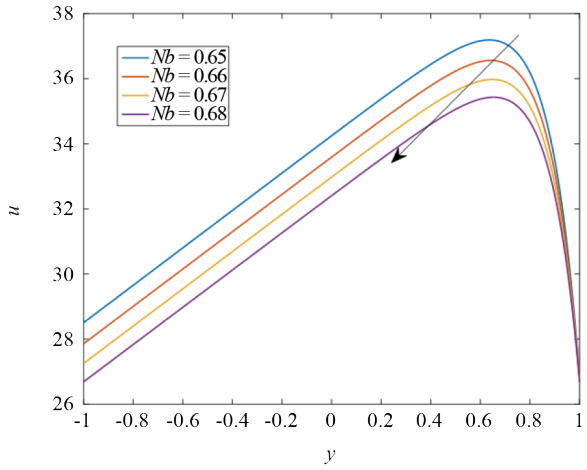

Figure 10. The difference in velocity for various Nb with $\phi = 0.10$, $Nt = 0.08$, $Nr = 0.25$, $k = 0.5$, $\lambda_1 = 0.6$

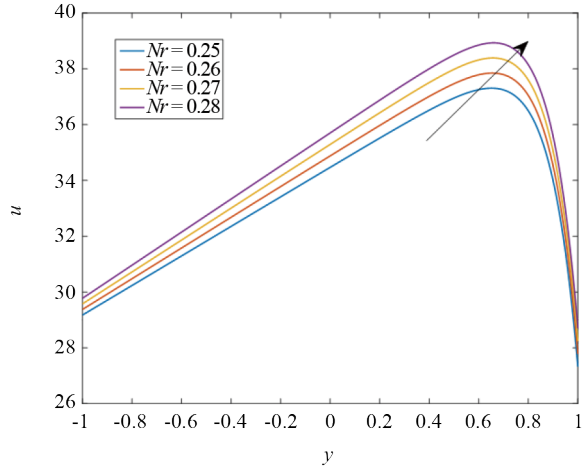

Figure 11. The difference in velocity for various Nr with $\phi = 0.10$, $Nt = 0.08$, $Nb = 0.68$, $k = 0.6$, $\lambda_1 = 0.6$

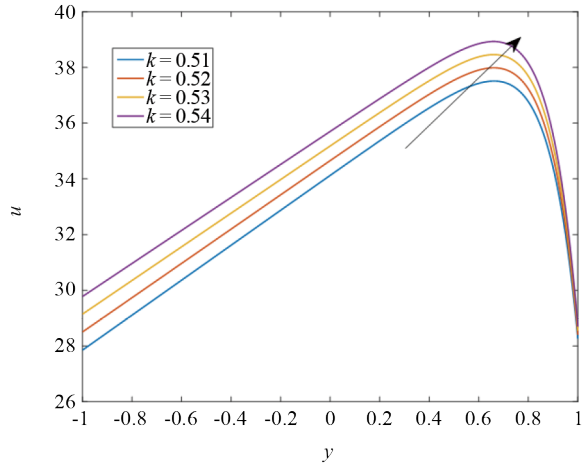

Figure 12. The difference in velocity for various k with $\phi = 0.10$, $Nt = 0.08$, $Nb = 0.68$, $Nr = 0.28$, $\lambda_1 = 0.6$

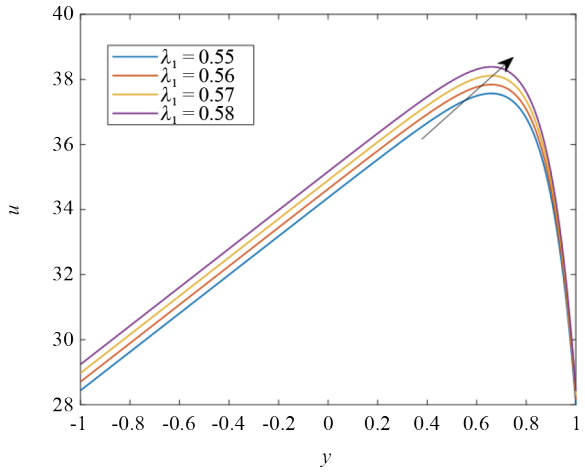

Figure 13. The difference in velocity fot various λ_1 with $\phi = 0.10$, $Nt = 0.08$, $Nb = 0.68$, $Nr = 0.28$, $k = 0.54$

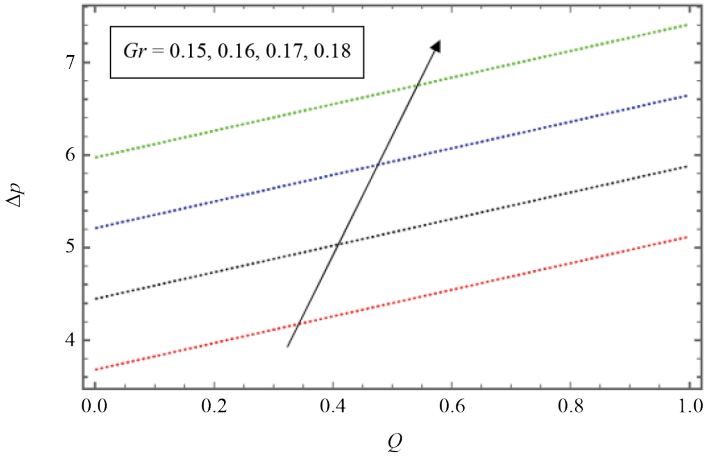

Figure 14. The difference of Δp with Q for various Gr with $\phi = 0.45$, $Nt = 0.40$, $Nb = 0.88$, $Re = 0.25$, $\lambda_1 = 0.75$, $k = 0.35$, $Nr = 0.65$

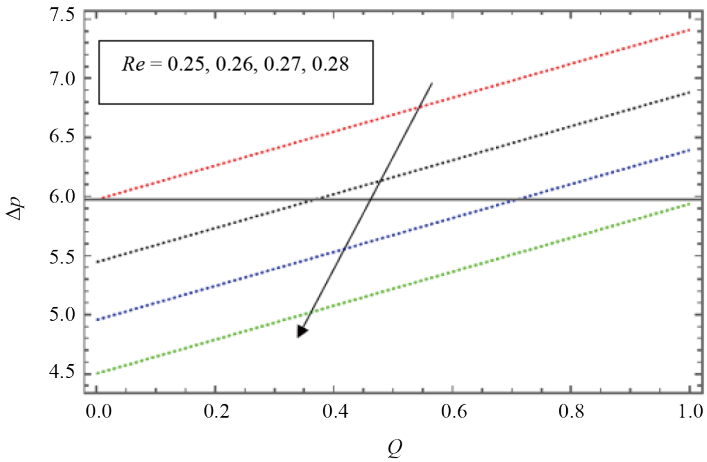

Figure 15. The difference of Δp with Q for various Re with $\phi = 0.45$, $Nt = 0.40$, $Nb = 0.88$, $\lambda_1 = 0.75$, $k = 0.35$, $Nr = 0.65$

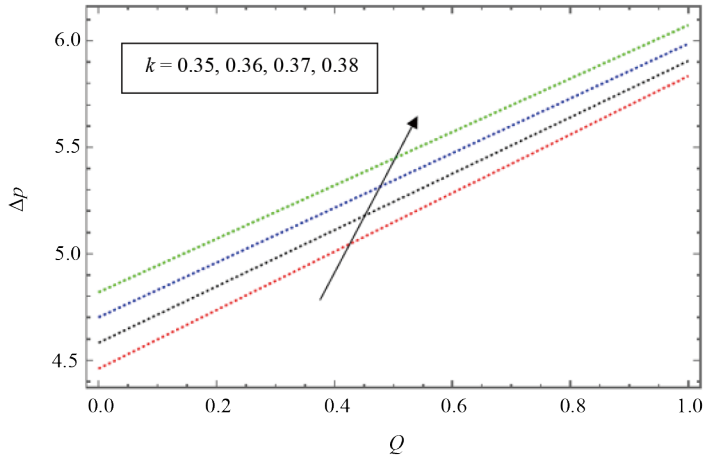

Figure 16. The difference of Δp with Q for various k with $\phi = 0.45$, $Nt = 0.40$, $Nb = 0.88$, $Re = 0.28$, $\lambda_1 = 0.78$, $Nr = 0.65$

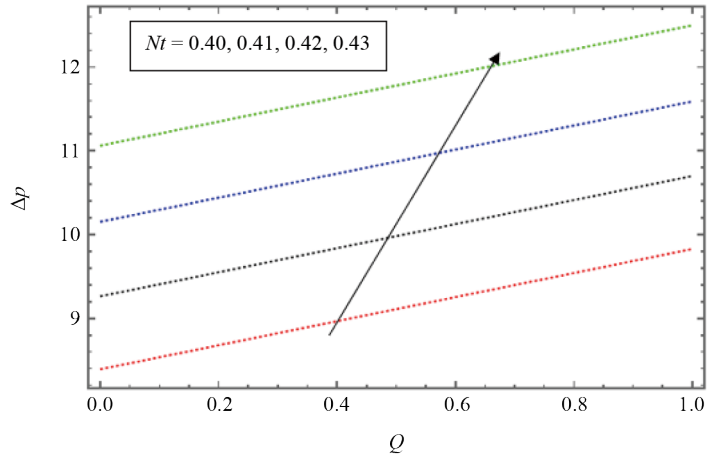

Figure 17. The difference of Δp with Q for various Nt with $\phi = 0.45$, $Nb = 0.85$, $Re = 0.68$, $Gr = 0.18$, $\lambda_1 = 0.75$, $k = 0.35$, $Nr = 0.65$

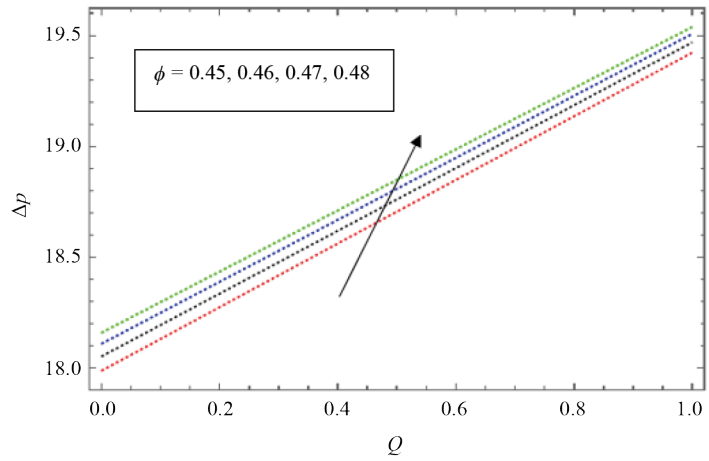

Figure 18. The difference of Δp with Q for various ϕ with $Nt = 0.50$, $Nb = 0.85$, $Gr = 0.45$, $Re = 0.68$, $\lambda_1 = 0.75$, $k = 0.35$, $Nr = 0.65$

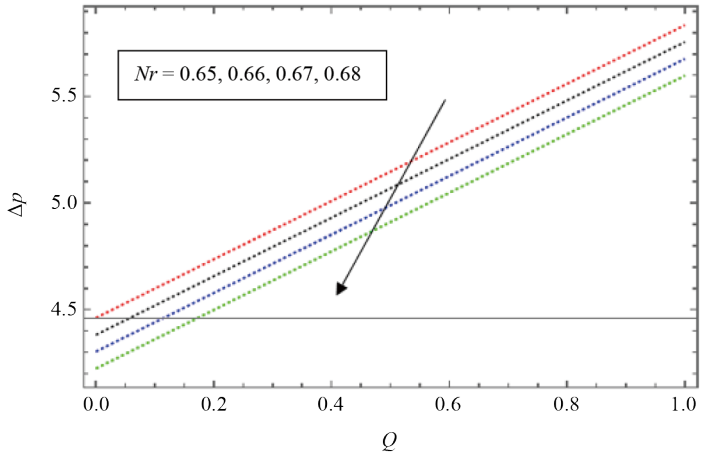

Figure 19. The difference of Δp with Q for various Nr with $\phi = 0.45$, $Nt = 0.40$, $Nb = 0.88$, $Gr = 0.18$, $Re = 0.28$, $\lambda_1 = 0.78$, $k = 0.35$, $Nr = 0.65$

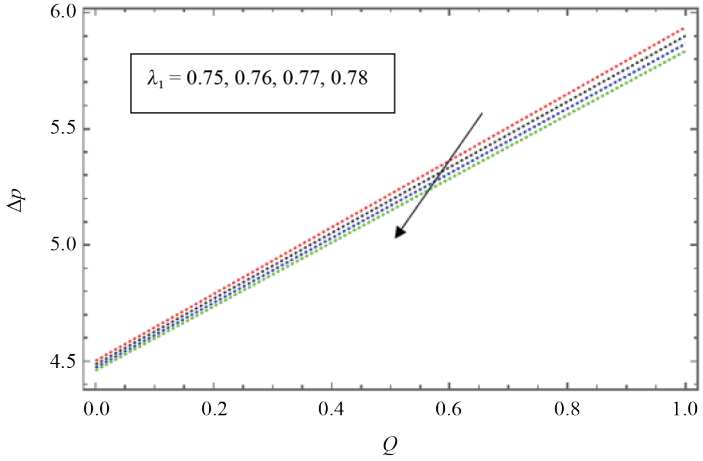

Figure 20. The difference of Δp with Q for various λ_1 with $\phi = 0.45$, $Nt = 0.40$, $Nb = 0.88$, $Gr = 0.18$, $Re = 0.28$, $k = 0.35$, $Nr = 0.65$

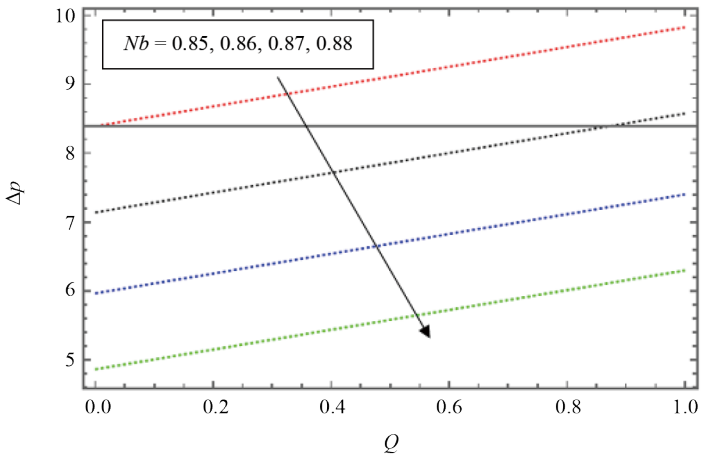

Figure 21. The difference of Δp with Q for various Nb with $\phi = 0.45$, $Nt = 0.40$, $Gr = 0.45$, $Re = 0.68$, $\lambda_1 = 0.75$, $k = 0.35$, $Nr = 0.65$

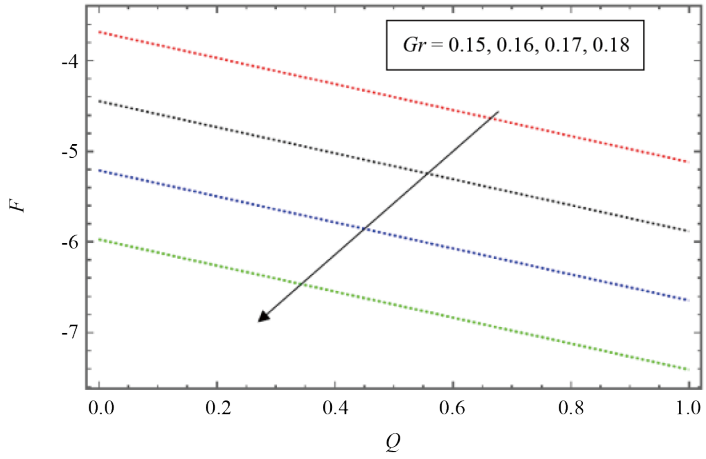

Figure 22. The difference of F with Q for various Gr with $\phi = 0.45$, $Nt = 0.40$, $Nb = 0.88$, $Re = 0.25$, $\lambda_1 = 0.75$, $k = 0.35$, $Nr = 0.65$

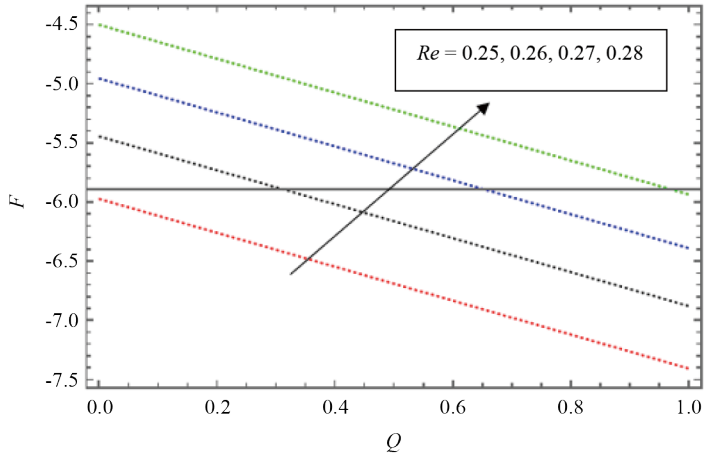

Figure 23. The difference of F with Q for various Re with $\phi = 0.45$, $Nt = 0.40$, $Nb = 0.88$, $\lambda_1 = 0.75$, $k = 0.35$, $Nr = 0.65$

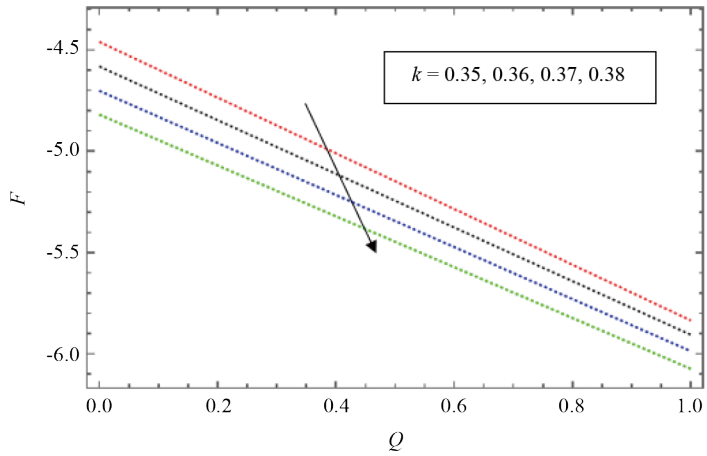

Figure 24. The difference of F with Q for various k with $\phi = 0.45$, $Nt = 0.40$, $Nb = 0.88$, $Re = 0.28$, $\lambda_1 = 0.78$, $Nr = 0.65$

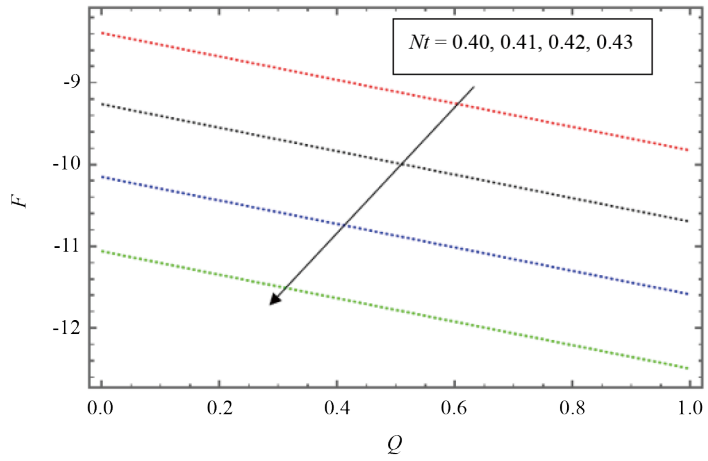

Figure 25. The difference of F with Q for various Nt with $\phi = 0.45$, $Nb = 0.85$, $Re = 0.68$, $Gr = 0.18$, $\lambda_1 = 0.75$, $k = 0.35$, $Nr = 0.65$

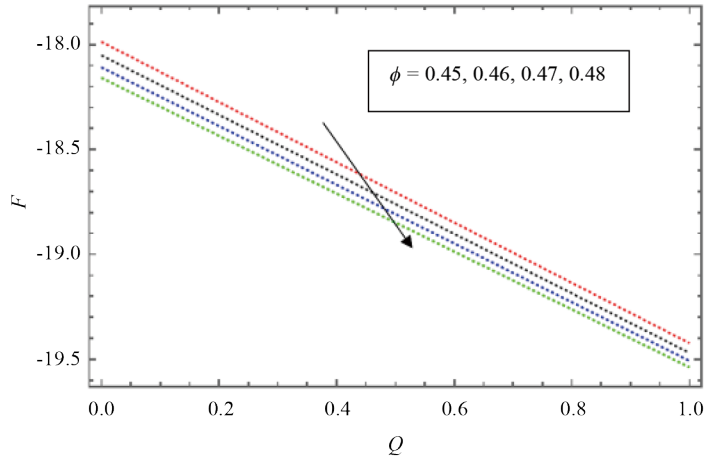

Figure 26. The difference of F with Q for various ϕ with $Nt = 0.50$, $Nb = 0.85$, $Gr = 0.45$, $Re = 0.68$, $\lambda_1 = 0.75$, $k = 0.35$, $Nr = 0.65$

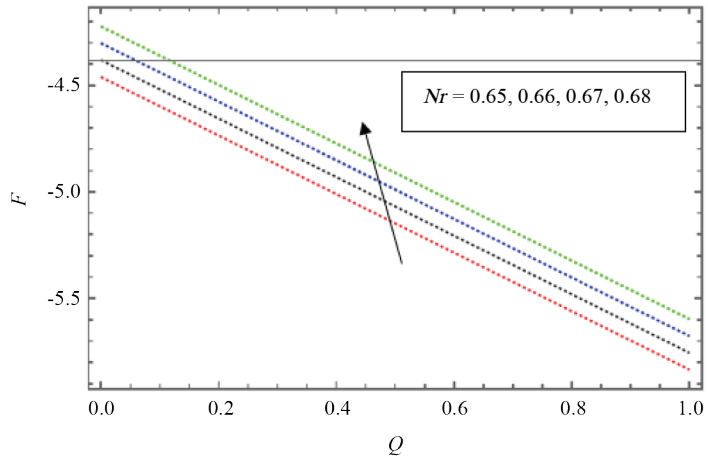

Figure 27. The difference of F with Q for various Nr with $\phi = 0.45$, $Nt = 0.40$, $Nb = 0.88$, $Gr = 0.18$, $Re = 0.28$, $\lambda_1 = 0.78$, $k = 0.35$, $Nr = 0.65$

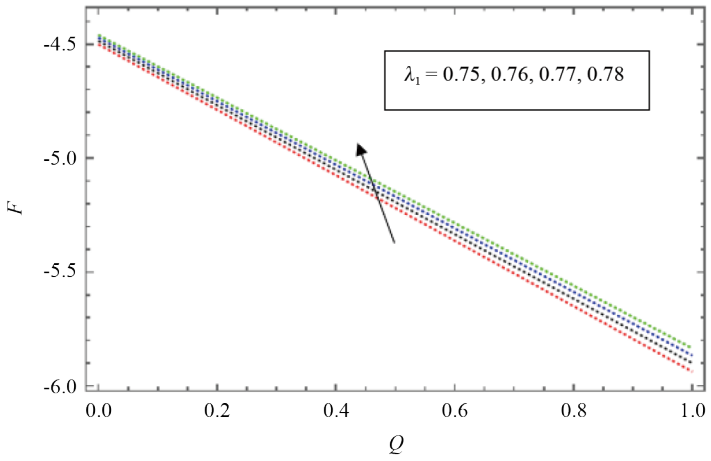

Figure 28. The difference of F with Q for various λ_1 with $\phi = 0.45$, $Nt = 0.40$, $Nb = 0.88$, $Gr = 0.18$, $Re = 0.28$, $k = 0.35$, $Nr = 0.65$

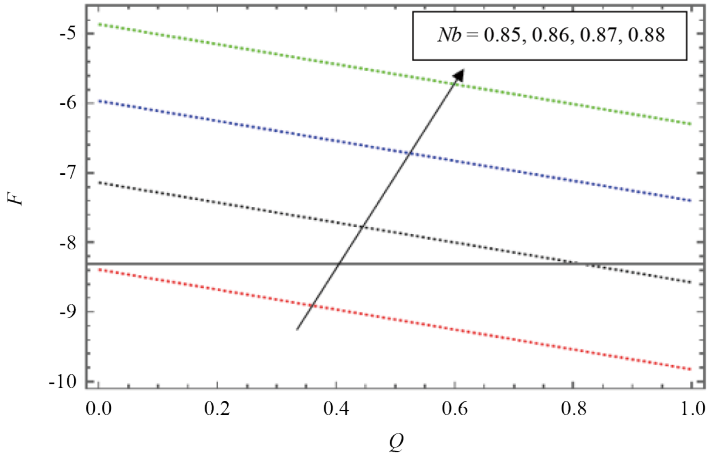

Figure 29. The difference of F with Q for various Nb with $\phi = 0.45$, $Nt = 0.40$, $Gr = 0.45$, $Re = 0.68$,$\lambda_1 = 0.75$, $k = 0.35$, $Nr = 0.65$

From Figure 14-21 illustrate how the pressure rate varies in relation to the mean flow for various physical term values. The mean flow increases together with a decreasing pressure rise. From Figure 15, 17 and 19 looks into how the pressure rate is affected by the buoyancy ratio, thermophoresis parameter and reynolds number. Although there are three possible pumping ranges, namely ($\Delta p > 0$) i.e., the pumping region, ($\Delta p = 0$) i.e., the free pumping region, ($\Delta p < 0$) i.e., the co-pumping region. On other hand Figure 14 demonstrates that the pressure rise dimnishes as the value of the grashof number terms increases. From Figure 15 and 19 demonstrates how the pressure rate enhances as Nr and Re value decreases. From Figure 16 shows the increasing the suction and injection parameter k values then the pressure rate also increases. From Figure 17 the pressure difference is strongly increased by increasing the thermophoresis parameter (Nt), which is of most interest in medical engineering. In this instance, the pattern holds constant for all averaged volume flow rate a values. In otherwords, a pressure difference decrease or rise can be maintained in nano peristaltic pumps at all working flow rates with an increasing thermophoresis effect. From Figure 18 displays the change in pressure rise for various amplitude values. It has been observed that the pressure increases as the value of ϕ increases. In Figure 20 while increasing the Jeffrey fluid parameter then the pressure rate is reduced. In Figure 21 shows that increasing the value for brownian motion parameter then the pressure rise also decreases. The fluctation in frictional force for various mean flow rate values of Gr, Re, k, ϕ, Nr, λ_1, Nb, Nt are depicted in Figure 22-29 respectievely. Frictional force is just opposite behaviour for the pressure rise.

6. Conclusion

The effect of suction and injection on the peristaltic mechanism of a Jeffrey nanofluid in a vertical tube is investigated. It is investigated how various physiological parameters are influenced by various parameters. The investigation is required to fully appreciate the issue. Examples of these flows are transpiration cooling, ultrafiltration in the glomerular tubules, fluid reabsorption through the porous walls of the renal proximal tube in the kidneys, and blood filtering during haemodialysis in an artificial kidney. The following are some of the noteworthy discoveries.

(1) It has been observed that velocity profile must be decreases in Amplitude ratio, brownian motion, then increases in, Buoyancy ratio, Thermophoresis parameter, suction and injection, λ_1.

(2) It demonstrated the concentration of nanoparticles increases in Brownian motion and decreases in Amplitude ratio, and Thermophoressis is parameter.

(3) It is observed that temperature profiles increases in all values Amplitude ratio, Thermoporesis, and Brownian motion parameter.

(4) The fluctation in pressure rise for various mean flow rate values of Gr, Re, k, ϕ, Nr, λ_1, Nb, Nt are depicted respectievely. In these Nt, k, Gr, ϕ those rising the parameter value then the pressure rise is increases and then pressure rise decreases in Re, λ_1, Nr, Nb.

(5) Frictional force is just opposite behavior of the pressure rise.

7. Application

In current analysis, considered the application of peristalsis phenomenon. How peristaltic transport is associated to the blood flow application. Peristaltic transport is often associated with blood flow applications due to its fundamental role in biological systems and its practical implications in medical and engineering contexts. Here's a detailed breakdown of why peristaltic transport is relevant to blood flow:

1. Biological Similarity Peristalsis in Biological Systems: Peristalsis is a type of wave-like muscle contraction that occurs in various tubular structures within the body, such as the digestive tract, ureters, and even blood vessels. It helps in moving contents through these tubes efficiently. Blood Flow Mechanics: The movement of blood through the circulatory system shares similarities with peristaltic transport. The arteries and veins exhibit pulsatile flow patterns due to the rhythmic contraction of the heart and the surrounding smooth muscle. Understanding peristaltic flow helps in modeling and analyzing these pulsatile characteristics.

2. Flow Characteristics Wave Propagation: Peristaltic transport involves wave propagation, which is also a key characteristic of blood flow. The pressure and velocity profiles in peristaltic flow can be analogous to the pressure wave and velocity variations observed in arterial blood flow. Efficiency and Transport: Peristaltic transport is highly efficient in transporting fluids with minimal energy loss. This principle can be applied to understanding how blood is propelled through the cardiovascular system, especially in pathological conditions where peristaltic-like mechanisms might be involved in compensatory strategies.

3. Medical and Engineering Applications Medical Devices: Peristaltic pumps, which operate on the principle of peristalsis, are used in various medical devices to move fluids with precision, such as in dialysis machines, infusion pumps, and in some cardiovascular devices. Understanding peristaltic flow is crucial for optimizing these devices' performance. Diagnostic and Therapeutic Insights: Studying peristaltic transport can provide insights into how irregularities in peristalsis might affect blood flow, leading to conditions like varicose veins or other vascular diseases. It also helps in designing interventions or treatments that mimic or enhance natural peristaltic actions.

4. Theoretical Modeling Flow Models: Mathematical and computational models of peristaltic transport can be adapted to simulate blood flow dynamics. These models help in understanding complex interactions within the circulatory system, including how changes in vessel geometry, elasticity, and fluid properties influence blood movement. The association of peristaltic transport with blood flow applications arises from the shared principles of wave-like motion and fluid transport efficiency. By leveraging the understanding of peristalsis, researchers and engineers can improve medical devices, enhance diagnostic methods, and develop treatments for vascular conditions.

Author contribution

Each author has made an equal contribution to this paper.

Data availability

Data sharing is not relavent to this article since no datasets were produced or analyzed in the current study.

Conflict of interest

The author declares no conflict of interest.

References

[1] Akbar NS, Nadeem S. Mixed convective magnetohydrodynamic peristaltic flow of a Jeffrey nanofluid with Newtonian heating. *Zeitschrift fur Naturforschung A*. 2013; 68(6-7): 433-441. Available from: https://doi.org/10.5560/zna.2013-0029.

[2] Reddy MS, Rao AR, Sreenadh S. Peristaltic motion of a power-law fluid in an asymmetric channel. *International Journal of Non-Linear Mechanics*. 2007; 42(10): 1153-1161. Available from: https://doi.org/10.1016/j.ijnonlinmec.2007.08.003.

[3] Weinberg SL. *A Theoretical and Experimental Treatment of Peristaltic Pumping and Its Relation to Ureteral Function*. Cambridge: Massachusetts Institute of Technology; 1970.

[4] Berman AS. Laminar flow in channels with porous walls. *Journal of Applied Physics*. 1956; 27(12): 1557-1562.

[5] Mishra M, Rao AR. Peristaltic transport in a channel with a porous peripheral layer: model of a flow in gastrointestinal tract. *Journal of Biomechanics*. 2005; 38(4): 779-789. Available from: https://doi.org/10.1016/j.jbiomech.2004.05.017.

[6] Noreen S, Hayat T, Alsaedi A. Study of slip and induced magnetic field on the peristaltic flow of pseudoplastic fluid. *International Journal of Physical Sciences*. 2011; 6(36): 8018-8026.

[7] Channabasappa MN, Umapathy KG, Nayak IV. Effect of porous lining on the flow between two concentric rotating cylinders. *Proceedings of the Indian Academy of Sciences-Mathematical Sciences*. 1979; 88: 63-167. Available from: https://doi.org/10.1007/BF02871613.

[8] Usman H, Magami MS, Ibrahim M, Omokhuale E. Combined effects of magnetic field and chemical reaction on unsteady natural convective flow in a vertical porous channel. *Asian Journal of Mathematics and Computer Research*. 2017; 19(2): 87-100.

[9] Shojaefar MH, Noorpoor AR, Avanesians A, Ghaffarpou M. Numerical investigation of flow control by suction and injection on a subsonic airfoil. *American Journal of Applied Sciences*. 2005; 2(10): 1474-1480. Available from: https://doi.org/10.3844/ajassp.2005.1474.1480.

[10] Brasseur JG, Corrsin S, Lu NQ. The influence of a peripheral layer of different viscosity on peristaltic pumping with Newtonian fluids. *Journal of Fluid Mechanics*. 1987; 174: 495-519. Available from: https://doi.org/10.1017/S0022112087000211.

[11] Chandra P, Prasad JK. Pulsatile flow in circular tubes of varying cross-section with suction/injection. *The ANZIAM Journal*. 1994; 35(3): 366-381. Available from: https://doi.org/10.1017/S0334270000009358.

[12] Qadeer M, Khan U, Ahmad S, Ullah B, Mousa M, Khan I. Irreversibility analysis for flow of nanofluids with aggregation in converging and diverging channel. *Scientific Reports*. 2022; 12(1): 10214. Available from: https://doi.org/10.1038/s41598-022-14529-8.

[13] Kumar KG, Rahimi-Gorji M, Reddy MG, Chamkha AJ, Alarifi IM. Enhancement of heat transfer in a convergent/divergent channel by using carbon nanotubes in the presence of a Darcy-Forchheimer medium. *Microsystem Technologies*. 2020; 26: 323-332. Available from: https://doi.org/10.1007/s00542-019-04489-x.

[14] Anuar NS, Bachok N, Arifin NM, Rosali H. Effect of suction/injection on stagnation point flow of hybrid nanofluid over an exponentially shrinking sheet with stability analysis. *CFD Letters*. 2019; 11(12): 21-33.

[15] Rasool G, Shafiq A, Durur H. Darcy-Forchheimer relation in Magnetohydrodynamic Jeffrey nanofluid flow over stretching surface. *Discrete and Continuous Dynamical Systems-Series S*. 2021; 14(7): 2497-2515. Available from: https://doi.org/10.3934/dcdss.2020399.

[16] Swain BK, Parida BC, Kar S, Senapati N. Viscous dissipation and joule heating effect on MHD flow and heat transfer past a stretching sheet embedded in a porous medium. *Heliyon*. 2020; 6(10): e05338. Available from: https://doi.org/10.1016/j.heliyon.2020.e05338.

[17] Hussein SA, Ahmed SE, Arafa AA. Electrokinetic peristaltic bioconvective Jeffrey nanofluid flow with activation energy for binary chemical reaction, radiation and variable fluid properties. *ZAMM-Journal of Applied Mathematics and Mechanics/Zeitschrift für Angewandte Mathematik und Mechanik*. 2023; 103(1): e202200284. Available from: https://doi.org/10.1002/zamm.202200284.

[18] Haseena C, Srinivas AN. Peristaltic transport of a nanofluid in a vertical channel. *Journal of Nanofluids*. 2017; 6(4): 624-636. Available from: https://doi.org/10.1166/jon.2017.1366.

[19] Tayebi T, El-Sapa S, Karimi N, Dogonchi AS, Chamkha AJ, Galal AM. Double-diffusive natural convection with Soret/Dufour effects and energy optimization of nano-encapsulated phase change material in a novel form of a wavy-walled I-shaped domain. *Journal of the Taiwan Institute of Chemical Engineers*. 2023; 148: 104873. Available from: https://doi.org/10.1016/j.jtice.2023.104873.

[20] Dogonchi AS, Waqas M, Afshar SR, Seyyedi SM, Hashemi-Tilehnoee M, Chamkha AJ, et al. Investigation of magneto-hydrodynamic fluid squeezed between two parallel disks by considering Joule heating, thermal radiation, and adding different nanoparticles. *International Journal of Numerical Methods for Heat and Fluid Flow*. 2020; 30(2): 659-680. Available from: https://doi.org/10.1108/HFF-05-2019-0390.

[21] Tirth V, Pasha AA, Tayebi T, Dogonchi AS, Irshad K, Chamka AJ, et al. Efficacy of exothermic reaction on the thermal-free convection in a nanoencapsulated phase change materials-loaded enclosure with circular cylinders inside. *Case Studies in Thermal Engineering*. 2023; 45: 102942. Available from: https://doi.org/10.1016/j.est.2022.106522.

[22] Nayak MK, Dogonchi AS, Rahbari A. Free convection of Al_2O_3-water nanofluid inside a hexagonal-shaped enclosure with cold diamond-shaped obstacles and periodic magnetic field. *Case Studies in Thermal Engineering*. 2023; 50: 103429. Available from: https://doi.org/10.1016/j.csite.2023.103429.

[23] Dogonchi AS, Bondareva NS, Sheremet MA, El-Sapa S, Chamkha AJ, Shah NA. Entropy generation and heat transfer performance analysis of a non-Newtonian NEPCM in an inclined chamber with complicated heater inside. *Journal of Energy Storage*. 2023; 72: 108745. Available from: https://doi.org/10.1016/j.est.2023.108745.

[24] Rafiq M, Sajid M, Alhazmi SE, Khan MI, El-Zahar ER. MHD electroosmotic peristaltic flow of Jeffrey nanofluid with slip conditions and chemical reaction. *Alexandria Engineering Journal*. 2022; 61(12): 9977-9992. Available from: https://doi.org/10.1016/j.aej.2022.03.035.

[25] Pasha AA, Alam MM, Tayebi T, Kasim S, Dogonchi AS, Irshad K, et al. Heat transfer and irreversibility evaluation of non-Newtonian nanofluid density-driven convection within a hexagonal-shaped domain influenced by an inclined magnetic field. *Case Studies in Thermal Engineering*. 2023; 41: 102588. Available from: https://doi.org/10.1016/j.csite.2022.102588.

[26] Seyyedi SM, Hashemi-Tilehnoee M, Del Barrio EP, Dogonchi AS, Sharifpur M. Analysis of magneto-natural-convection flow in a semi-annulus enclosure filled with a micropolar-nanofluid; a computational framework using CVFEM and FVM. *Journal of Magnetism and Magnetic Materials*. 2023; 568: 170407. Available from: https://doi.org/10.1016/j.jmmm.2023.170407.

[27] Pasha AA, Tayebi T, MottahirAlam M, Irshad K, Dogonchi AS, Chamkha AJ, et al. Efficacy of exothermic reaction on the thermal-free convection in a nano-encapsulated phase change materials-loaded enclosure with circular cylinders inside. *Journal of Energy Storage*. 2023; 59: 106522. Available from: https://doi.org/10.1016/j.est.2022.106522.

[28] Abd-Alla AM, Abo-Dahab SM, Abdelhafez MA, Thabet EN. Effects of heat transfer and the endoscope on Jeffrey fluid peristaltic flow in tubes. *Multidiscipline Modeling in Materials and Structures*. 2021; 17(5): 895-914. Available from: https://doi.org/10.1108/MMMS-12-2020-0292.

[29] Shao Y, Nayak MK, Dogonchi AS, Chamkha AJ, Elmasry Y, Galal AM. Ternary hybrid nanofluid natural convection within a porous prismatic enclosure with two movable hot baffles: An approach to effective cooling. *Case Studies in Thermal Engineering*. 2022; 40: 102507. Available from: https://doi.org/10.1016/j.csite.2022.102507.

[30] Li X, Abbasi A, Al-Khaled K, Ameen HF, Khan SU, Khan MI, et al. Thermal performance of iron oxide and copper (Fe_3O_4, Cu) in hybrid nanofluid flow of Casson material with Hall current via complex wavy channel. *Materials Science and Engineering: B*. 2023; 289: 116250. Available from: https://doi.org/10.1016/j.mseb.2022.116250.

[31] Bafakeeh OT, Al-Khaled K, Khan SU, Abbasi A, Ganteda C, Khan MI, et al. On the bioconvective aspect of viscoelastic micropolar nanofluid referring to variable thermal conductivity and thermo-diffusion characteristics. *Bioengineering*. 2023; 10(1): 73. Available from: https://doi.org/10.3390/bioengineering10010073.

[32] Turkyilmazoglu M. Corrections to long wavelength approximation of peristalsis viscous fluid flow within a wavy channel. *Chinese Journal of Physics*. 2024; 89: 340-354. Available from: https://doi.org/10.1016/j.cjph.2024.03.030.

[33] Rahman M, Sharif F, Turkyilmazoglu M, Siddiqui MS. Unsteady three-dimensional magnetohydrodynamics flow of nanofluids over a decelerated rotating disk with uniform suction. *Pramana*. 2022; 96(4): 170. Available from: https://doi.org/10.1007/s12043-022-02404-0.

[34] Siddiqui AA, Turkyilmazoglu M. Film flow of nano-micropolar fluid with dissipation effect. *CMES-Computer Modeling in Engineering and Sciences*. 2024; 140(3): 2487-2512. Available from: https://doi.org/10.32604/cmes.2024.050525.

[35] Gayathri R, Srinivas S, Kothandapani M. The influence of slip conditions, wall properties and heat transfer on MHD peristaltic transport. *Computer Physics Communications*. 2009; 180(11): 2115-2122. Available from: https://doi.org/10.1016/j.cpc.2009.06.015.

[36] Srinivas AN, Haseena C, Sreenadh S. Peristaltic transport of nanofluid in a vertical porous stratum with heat transfer effects. *BioNanoScience*. 2019; 9: 117-130. Available from: https://doi.org/10.1007/s12668-018-0571-y.